

# GM1 Softens POPC Membranes and Induces the Formation of Micron-Sized Domains

Nico Fricke<sup>1</sup> and Rumiana Dimova<sup>1,\*</sup>

<sup>1</sup>Max Planck Institute of Colloids and Interfaces, Science Park Golm, Potsdam, Germany

**ABSTRACT** The influence of the glycolipid GM1 on the physical properties of POPC membranes was studied systematically by using different methods applied to giant and large unilamellar vesicles. The charge per GM1 molecule in the membrane was estimated from electrophoretic mobility measurements. Optical microscopy and differential scanning calorimetry were employed to construct a partial phase diagram of the GM1/POPC system. At room temperature, phase separation in the membrane was detected for GM1 fractions at and above ~5 mol %, whereby GM1-rich gel-like domains were observed by fluorescent microscopy. Fluctuation analysis, vesicle electrodeformation, and micropipette aspiration were used to assess the bending rigidity of the membrane as a function of GM1 content. In the fluid phase, GM1 was shown to strongly soften the bilayer. In the region of coexistence of fluid and gel-like domains, the micropipette aspiration technique allowed measurements of the bending rigidity of the fluid phase only, whereas electrodeformation and fluctuation analysis were affected by the presence of the gel-phase domains. The observation that GM1 decreased the bilayer bending rigidity is important for understanding the role of this ganglioside in the flexibility of neuronal membranes.

## INTRODUCTION

Glycolipids are important components in the outer leaflet of biological membranes. They get increasingly in the focus of membrane research as new processes for synthesizing glycolipids emerge (1) and new applications in immunotherapy are discovered (2). Similarly to phospholipids, glycolipids consist of fatty acids, which are bound to a glycerin backbone but carry a sugar or a sugar chain as a headgroup. The glycosphingolipids are present as a minor component in mammalian cells and are localized almost exclusively at the external leaflet of the plasma membrane (3). They are abundant in the central nervous system (3) and play a significant role in the modulation of cell functionality, recognition, and adhesion (4–6). Although they are a minor component, they constitute 5–10% of the total lipid mass in nerve cells (7) (corresponding to 10–20 mol % of the outer leaflet of the cell membrane).

Gangliosides are glycolipids with sphingosine as the base and at least one negatively charged sialic acid group. The glycolipid GM1, the prototype of gangliosides, consists of four sugar groups and one sialic acid residue in the headgroup and a hydrophobic ceramide moiety. It is probably one of the

most commonly studied gangliosides. An extensive review of the physicochemical and structural behaviors of GM1 can be found in Ref. (8). It acts as a natural plasma membrane receptor for cholera toxin. GM1 plays a crucial role in connection with receptor proteins for cell-cell communication and can be found at high concentrations in the central nervous system of mammals. It strongly influences neural plasticity (4), was recently recognized as a factor in slowing down the progression of Parkinson disease (9), and is involved in a large number of essential functions in the plasma membrane and intracellular loci (for a recent review, see Ref. (10)). Probably the most widely accepted understanding about the role of GM1 is that the most important functions of this ganglioside are ensured predominantly via binding to proteins. However, the manifold functionality of this ganglioside is now being recognized (10). The complexity of ganglioside involvement can be understood not only from studies of their interactions with proteins and structural metamorphism but also from physicochemical data regarding their contributions to demixing and cooperativity (11). As we will see in this work, GM1 molecules tend to segregate and in this way locally modulate the morphology and mechanics of the membrane, while their presence in the fluid membrane, even at small fractions, dramatically changes its bending rigidity.

Because GM1 is an important component of biological membranes, and in particular the nervous system, it is

Submitted March 7, 2016, and accepted for publication September 22, 2016.

\*Correspondence: [rumiana.dimova@mpikg.mpg.de](mailto:rumiana.dimova@mpikg.mpg.de)

Editor: Tobias Baumgart.

<http://dx.doi.org/10.1016/j.bpj.2016.09.028>

© 2016 Biophysical Society.

This is an open access article under the CC BY-NC-ND license (<http://creativecommons.org/licenses/by-nc-nd/4.0/>).



valuable to understand its effect on the physical characteristics of membranes. In particular, its elastic and thermodynamic properties play a significant role, since GM1 is known to be involved in neuronal development and differentiation (10,12) and neurite sprouting (13). To assess the effect of GM1 on the physicochemical properties of membranes, we used giant unilamellar vesicles (GUVs) as a model system (14,15). The phospholipid palmitoyl-oleoyl-phosphatidylcholine (POPC) was chosen as the forming lipid.

To characterize the influence of GM1 on the bending rigidity of the membrane, we applied the well-established methods of fluctuation spectroscopy (16–18) and micropipette aspiration (18–20). In addition, the method of vesicle electrodeformation (17,21,22) was used and a simplified approach for analyzing the data was proposed and applied. The membrane phase state of vesicles with varied GM1 content was characterized by fluorescence microscopy to build a partial phase diagram of the POPC/GM1 binary mixture.

## MATERIALS AND METHODS

### Vesicle preparation

GUVs were prepared using the electroformation method (23) with slight modifications as described below. POPC and GM1 ganglioside were dissolved in a dichloromethane/methanol (2:1) solution at a concentration of ~3 mM. Both lipids were purchased from Avanti Polar Lipids (Alabaster, AL). For fluorescence imaging, Texas Red dihexadecanoyl-glycerophosphoethanolamine (TR-DHPE) and/or Bodipy FL C5-ganglioside GM1 (Bodipy-GM1) (both from Invitrogen/Molecular Probes, Carlsbad, CA) were added at a total lipid concentration of 0.1 mol %. Cholera toxin B (CTB) labeled with Alexa 488 (CTB-Alexa) was purchased from Invitrogen.

The lipid solution (~20  $\mu$ L) was placed on two indium-tin-oxide-coated glass plates and dried under vacuum at 40°C for 2 h to remove the organic solvents. Both coated glass plates, with a 2-mm-thick Teflon frame, were assembled together to form a chamber held by clamps. After an electric AC field (0.2 V, 10 Hz, sinusoidal wave) was applied, ~2.2 mL of 1 mM HEPES buffer (pH = 7.4, 0.5 Na HEPES; Sigma-Aldrich, St. Louis, MO) was added. The voltage was linearly increased to 1.0 V in the first 40 min. The applied voltage was then kept constant for 30 min. To separate the GUVs from the indium-tin-oxide-coated surface, in the last 30 min, the voltage and frequency were linearly lowered to 0.5 V and 1 Hz. This adaptation of the electroformation protocol was found to be suitable for growing large GUVs from GM1-doped POPC bilayers. Afterward, the vesicles were transferred with a Pasteur pipette into the corresponding observation chambers for further investigation.

Both lipid drying and electrosweating were conducted at a temperature of 40°C, where the lipid bilayer is in the fluid state (as found in this study). Using this protocol, GUVs with a total GM1 fraction of up to 10% could be prepared. Higher fractions yielded no suitable GUVs (the yield was small, and the vesicles were not large and defect free). To prevent presumable interactions between sugars and GM1-doped membranes (for example, mediated by hydrogen bonding between sugars and lipids (24) and between sugars and alike GM1 headgroups), all measurements on GUVs were done without the conventional addition of sugars to create sucrose/glucose asymmetry for density gradient or optical contrast. Note that sugar-membrane interactions are known to affect the membrane bending rigidity (25,26).

Large unilamellar vesicles (LUVs) were prepared by extrusion. First, lipids from the same stock solution used for the electroformation protocol

were dried on the bottom of a glass vial for 2–3 h under vacuum at 40°C. After the buffer solution was added and the vial was shaken for 30 min, the obtained vesicle suspension was extruded through polycarbonate membranes with pore diameters of 400 nm, 200 nm, and finally 100 nm, 20 times each, at 40–45°C. The average diameter of the LUVs at a lipid concentration of 2 mM in the final suspension was (115  $\pm$  7) nm. The size distribution of the vesicles was measured using dynamic light scattering (Zetasizer Nano ZS; Malvern Instruments, Worcestershire, UK).

### Fluctuation analysis

Fluctuation analysis was performed according to the protocol described in Ref. (17). The GUVs were placed in a chamber made of two coverslips and a 2-mm-thick ring made of Teflon, and observed under phase contrast. The temperature of the sample was regulated by a heating bath. Several thousand snapshots were acquired with a high-speed digital camera (HG-100 K; Redlake, San Diego, CA) or a high-resolution camera (pco.edge; PCO AG, Kelheim, Germany) at a frequency of 125–250 frames per second (no dependence on the acquisition frequency was observed) and the image exposure time was set between 100 and 200  $\mu$ s. Since the intra- and extra-vesicular solutions were identical, the influence of gravity on the fluctuation spectra could be excluded (27). Here, more than 15 vesicles per membrane composition were examined.

### Micropipette aspiration

The GUVs were placed in a chamber with a horse-shoe-shaped spacer made of Teflon. Micropipettes with inner tip diameters between 7 and 15  $\mu$ m were prepared using a pipette puller (Sutter Instruments, Novato, CA) and their tips were shaped with a microforge (Narishige, Tokyo, Japan). The pipettes were connected to a water reservoir located on a height-adjustable precision linear stage (M531.21; Physik Instrumente, Karlsruhe, Germany), providing control of the pressure  $P$  at the pipette tip (see Ref. (18) for more details on the setup). Quantitative optical detection of the vesicle radii  $R_{ves}$ , the pipette radii  $R_{pip}$ , and the length of the aspirated part of the vesicle was done using a confocal laser scanning microscope (TCS SP5; Leica, Mannheim, Germany). The membrane tension was determined as  $\Sigma = PR_{pip}/[2(1 - R_{pip}/R_{ves})]$  (28). Changes in the projected membrane surface area  $\alpha$  were evaluated considering a quasi-constant volume (20). The projected surface  $A_{mem}$  of a GUV increases with tension  $\Sigma$ , and, for low tensions, the additional area stored in the membrane fluctuations has a dominant contribution (19,29), yielding for the relative area change:

$$\alpha \equiv \frac{\Delta A_{mem}}{A_{mem}^0} \approx \frac{k_B T}{8\pi\kappa} \ln\left(\frac{\Sigma}{\Sigma_0^*}\right), \quad (1)$$

where  $A_{mem}^0$  is the initial surface area of the vesicle,  $k_B$  is the Boltzmann constant,  $T$  is the temperature, and  $\Sigma_0^*$  is the effective membrane tension.

Adhesion of the vesicle membrane onto the pipette was partially suppressed by coating the pipettes with bovine serum albumin (Sigma-Aldrich). Rupturing a GUV with the bare pipette before performing a measurement appeared to be a more efficient way to coat the pipette. Typically, the vesicles possessed significant excess area, which consistently led to budding of the aspirated vesicles into the pipette at higher tensions. This behavior hindered measurements in the stretching-dominated regime. Thus, the data were collected at low tensions, where the apparent membrane area increases as a result of smoothing the membrane undulations (Eq. 1). Osmotic stabilization by using sugar solutions of osmolarities on the order of 100 mOsm is typically done to ensure that no vesicles leak during the application of suction pressure in aspiration measurements. Because of the lack of strong osmotic stabilization in our experiments, we were concerned about a loss of vesicle volume during aspiration. We were able to overcome this problem by performing the measurements relatively quickly. The waiting time between the applied pressure steps (corresponding to an

~0.01 mN/m change in vesicle tension for the entropic regime) was set to 3–5 s. This time appeared to be sufficient to achieve equilibration, judging from the negligible hysteresis observed when we performed the measurements while increasing or decreasing the pressure.

## Simplified analysis for vesicle electrodeformation

Vesicle electrodeformation as means of deducing the bending rigidity of membranes was introduced by Kummrow and Helfrich (21) and Niggemann et al. (22), and later was further developed by our group (17). Briefly, a selected vesicle is subjected to an AC electric field with a frequency of 2 kHz and increasing strength. The induced deformation of the vesicle shape is recorded. The field increases the tension of the membrane. The tension can be assessed in the following way: the force density  $f$  arising from the accumulation of electric charge at both interfaces of the membrane acts as a local pressure on the membrane in addition to the pressure difference  $\Delta p$  between the interior and exterior of the vesicles, as described by the Young-Laplace equation. At the poles (pol) and the equator (equ), the force balance between pressure and tension has the form  $2M_{pol}\Sigma = \Delta p + f_{pol}$  and  $2M_{equ}\Sigma = \Delta p + f_{equ}$ , where  $M_{pol}$  and  $M_{equ}$  are the mean curvatures of the membrane at the poles and equator, respectively, and  $f_{pol}$  and  $f_{equ}$  are the respective force densities. By eliminating the osmotic pressure from these two equations, one can determine the membrane tension  $\Sigma$  of the vesicle.

A full theoretical description of the force densities acting on the vesicle membrane was derived in Ref. (30). Basically, they depend quadratically on the applied electric field strength,  $E_0$ . All other parameters that influence the force densities (such as permittivities, inner and outer vesicle radius and membrane thickness, conductivities, and field frequency) are constant during the experiment. The membrane bending rigidity is deduced by applying very mild tensions to the membrane at which Eq. 1 holds. Because of this logarithmic dependence, all system parameters contribute only as a constant term to the change in area (see the [Supporting Material](#)):

$$\alpha = \frac{k_B T}{8\pi\kappa} \ln\left(\frac{E_0^2}{M_{equ} - M_{pol}}\right) + const. \quad (2)$$

Thus, simply plotting the logarithmic term in Eq. 2 as a function of the relative area change allows one to deduce the bending rigidity from the slope of the data. In this way, the cost of extensive calculations of the membrane tension (see Ref. (30) and [Supporting Material](#)) is eliminated, and only the applied electrical voltage and the two semiaxes of the deformed vesicles must be measured experimentally. Note that this type of analysis can be applied also to vesicles in solutions containing salt, but not at high salt concentrations where ions may adsorb and contribute excess charge on the membrane surface (31). Similarly, it is also not applicable to membranes containing charged lipids.

For the conditions explored in this work (field frequency and symmetric conductivity across the membrane), GUVs exposed to an AC field deform into prolates (see, e.g., Refs. (32,33)). To obtain the mean curvatures  $M_{pol}$  and  $M_{equ}$  of the deformed GUV at the poles and equator, we detected the contours of the vesicles using an in-house-written program (17) and fitted them to an ellipse to obtain both semiaxes and thus the curvatures as well as the vesicle area. Plotting the area change as a function of the applied electric field strength rescaled by the mean curvatures (in arbitrary units) yields the bending rigidity of the membrane according to Eq. 2 (see [Fig. S1](#) for an example measurement).

The vesicle radius determines the choice of applied voltage needed to achieve the desired range of weak membrane tensions. Typically, vesicles with radii between 10 and 20  $\mu\text{m}$  were studied and the applied field amplitudes were up to 15 kV/m.

For experimental realization of the electrodeformation measurements, we used a modified electrofusion chamber (Eppendorf, Hamburg, Germany). The chamber contained two parallel platinum wires spaced at 500  $\mu\text{m}$ . It was sealed by a coverslip and tempered by a thermal bath. The elec-

trical field was linearly increased (at a rate of ~40 mV/s) for 100 s and controlled by in-house-written software. No hysteresis in the membrane area change was detected upon an increase or decrease in the field strength, suggesting that the observed vesicle shapes were equilibrated. Due to the inhomogeneity of the electric field near the electrodes (34), the measurements were done in the center of the chamber. By applying an electrical field before the measurement, we were able to select the vesicles with the strongest deformation and thus the lowest native membrane tension,  $\Sigma_0$ . At the same time, this step was used to smooth out existing membrane defects resulting from the preparation (35,36).

## Differential scanning calorimetry

For differential scanning calorimetry (DSC), extruded LUVs at a total lipid concentration of 2 mM in 1 mM HEPES buffer were used. The measurements were performed with a VP-DSC scanning calorimeter (MicroCal, Northampton, MA). At least 15 temperature cycles in the range of 10–70°C were recorded. The cooling/heating rate was set to 20 K/h. Scans with multilamellar vesicles (not extruded but only vortexed) at a lipid concentration of 4.3 mM were also performed at a faster cooling/heating rate of 60 K/h.

## Electrophoresis

For electrophoretic measurements, a vesicle suspension with lipid concentration of 0.4 mM was placed in a Zetasizer Nano ZS (Malvern Instruments). To estimate the  $\zeta$  potential from the electric mobility  $\mu_e$  of the LUVs, we used the Smoluchowski approximation  $\zeta = (3\eta/2\epsilon\epsilon_0 f_H)\mu_e$ , where  $\eta$  denotes the solution viscosity,  $\epsilon$  is the relative permittivity of the solution,  $\epsilon_0$  is the dielectric permittivity of the vacuum, and  $f_H = 1.30$  is the Henry function for our system. For each membrane composition, measurements at 40°C with 100 subruns were conducted and averaged. From the  $\zeta$  potential, the surface potential  $\psi^S \approx \zeta e^{-\gamma_D z^*}$  could be estimated, where the Debye screening length for our system is  $\gamma_D^{-1} = 7.5$  nm and the shear plane distance  $z^* = 0.2$  nm (37,38). Then, the vesicle effective surface charge  $Q_{eff}$  was assessed (39) as  $Q_{eff} = \sqrt{8\pi\epsilon_0 C_{ion} R T} \sinh(e N_A \psi^S / 2RT)$ , where  $C_{ion}$  is the ionic strength,  $R$  is the gas constant,  $e$  is the elementary charge, and  $N_A$  is the Avogadro number.

## RESULTS AND DISCUSSION

### Surface charge of GM1-doped membranes

We first assessed the surface charge of GM1-doped POPC vesicles to confirm the incorporation of the ganglioside in the membrane. [Fig. 1](#) shows the dependence of the membrane surface charge as a function of GM1 content in the POPC bilayer at a temperature of 40°C, where the membrane is completely in the fluid phase (see below). Here, the electrophoretic mobilities of LUVs with diameters  $115 \pm 7$  nm are displayed. A nearly linear increase in electrophoretic mobility with increasing concentrations of GM1 is observed, indicating successful incorporation of the glycolipid into the POPC bilayer. At the highest GM1 fraction explored, the vesicles exhibit almost 1.5 times the electrophoretic mobility of the bare POPC vesicles, even though the five sugar groups of GM1 (see [Fig. 2](#)) are expected to decrease vesicle mobility via hydrodynamic drag (40).

From data obtained for the  $\zeta$  potential and the effective vesicle surface charge (see above), we could roughly assess

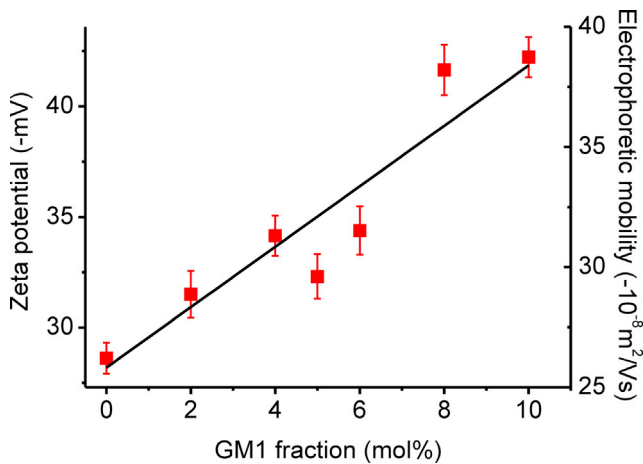


FIGURE 1 Influence of GM1 content on the electrophoretic mobility and  $\zeta$  potential of 2 mM POPC LUVs in 1 mM HEPES at 40°C. The error bars indicate standard error. To see this figure in color, go online.

the effective elementary charge per molecules in the membrane. Taking  $68 \text{ \AA}^2$  for the molecular area of POPC (41), we determined the charge per POPC molecule from the  $\zeta$  potential of GM1-free vesicles as  $\sim 0.01e$ , where  $e$  is the elementary charge. We then assumed that the POPC charge is constant for all lipid mixtures explored, and that the area per GM1 molecule is constant and between  $70 \text{ \AA}^2$  and  $85 \text{ \AA}^2$  (8). We thus obtained  $(0.076 \pm 0.003)e$  for the charge per GM1 molecule. The charge was found to be constant regardless of the membrane composition, corroborating the above assumptions. The small value for the charge of GM1 is

indicative of shielding or steric obstruction of the sialic acid residue by the bulky rest of the GM1 headgroup (see Fig. 2).

Although previous studies suggested that GM1 is thermodynamically more stable when incorporated into the membrane (3), we cannot exclude the possibility that a fraction of the GM1 molecules desorb in the bulk as either single molecules or micelles (literature values for the critical micellar concentration are quite scattered and in the range between  $10^{-10} \text{ M}$  and  $10^{-6} \text{ M}$  (42)). Indeed, as we discuss in an upcoming study (R. Dasgupta, N. Fricke, R. Lipowsky, and R. Dimova, unpublished data), diluting the vesicles after preparation results in desorption of GM1 from the outer leaflet, which changes the membrane spontaneous curvature. Here, no such dilution step was done.

### Phase diagram of GM1-doped POPC membranes and gel-like microdomains

Having characterized the membrane charge, we proceeded to study the thermodynamic properties and phase behavior of the GM1-doped membranes. The main phase transition temperature,  $T_m$ , of pure POPC is  $-4^\circ \text{ C}$ ; however, that of pure GM1 is not well defined since it strongly depends on the structural arrangement of the ganglioside and the preference to form micelles in aqueous solutions. The  $T_m$  values for GM1 are scattered between  $19^\circ \text{ C}$  and  $43^\circ \text{ C}$  (43). We investigated the phase behavior of POPC membranes doped with GM1 using DSC. For fractions below 5 mol %, there

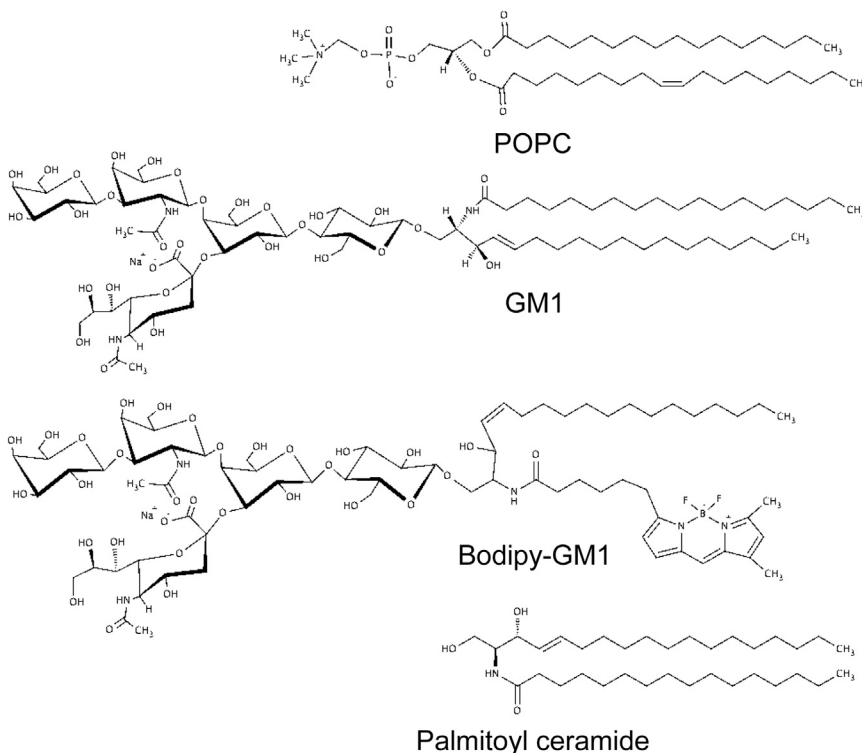


FIGURE 2 Chemical structures of POPC, GM1, Bodipy-GM1, and palmitoyl ceramide.

were no changes in the heat capacity, whereas for higher GM1 fractions, the position of the maxima appeared to vary strongly and depend on the baseline subtraction procedure. Thus, the data were considered unreliable to deduce the phase transition temperature. Presumably, the very low explored lipid concentration (up to 4.3 mM, corresponding to at most a 0.43 mM GM1 concentration) resulted in these inconclusive DSC traces. This outcome could be also a signature of a more complex transition than that observed between gel and fluid phases.

Even though no signature of phase separation was detected by DSC on LUVs, the formation of microscopic domains at room temperature could be observed on giant vesicles with GM1 fractions larger than 4 mol %. The temperatures at which the microdomains appeared upon cooling for other mixtures are presented in a partial phase diagram in Fig. 3 A. This study is probably the first to report the presence of such micron-sized domains in POPC membranes doped with GM1. Work using atomic force microscopy on supported POPC bilayers with varied fractions of GM1 did not report such phase separation on the micrometer scale, but did detect the presence of nanodomains with increasing size as a function of GM1 content (44). This discrepancy may result from differences in the explored systems, e.g., the supported bilayers (where mobility might be reduced) at high salt concentration examined in Ref. (44) versus the GUVs (i.e., freely suspended membranes) in low-saline buffer explored here. Note that phase diagrams of charged multicomponent membranes are sensitive to the presence of salt (45). We should also note that a large fraction of the GM1-doped vesicles (between 10% and 50%, with the higher fraction referring to membranes with a higher content of GM1) exhibited internal structures similar to those reported in (46) (see Fig. S2 for examples). For the imaging of domains, we selected clean vesicles with no such structures. The domains were visualized using

various fluorescent dyes. Fig. 3, B and C, show images of GUVs labeled with TR-DHPE. This fluorescent dye partitions almost exclusively in the liquid phase (47), suggesting that the dark domains represent a more ordered phase. These domains had a dendritic shape and could diffuse freely along the vesicle surface, indicating that the bright phase is fluid, but retained their shape and stiff boundaries, suggesting that they are gel like. The higher transition temperature of GM1 compared with POPC suggests that the bright fluid phase is POPC rich, whereas the gel-like dark domains are GM1 rich. Indeed, GM1 was previously reported to exert a condensing effect in single-component lipid monolayers (48), to form submicroscopic domains in supported membranes (49), and to partition into the gel phase of two-component supported bilayers (50) and multilamellar liposomes (51). It was also shown that GM1 prefers more ordered phases in multicomponent systems (47). A similar behavior is to be expected in the system examined here, i.e., a POPC-rich fluid phase and a GM1-rich gel-like phase.

The hydrophobic moieties of ceramides are similar to that of GM1 (see Fig. 2). Thus, when considering the phase behavior of GM1/POPC membranes as shown in Fig. 3 A, one can use ceramide/POPC systems as a frame of reference. Ceramides increase the molecular order in phospholipid membranes and have been shown to induce phase separation (52). The phase diagram of palmitoylceramide/POPC bilayers was characterized in detail in a previous study (53), which reported the formation of ceramide-rich gel-like domains. Despite the shorter carbon chain of palmitoyl ceramide, the liquidus line is slightly higher than the one we find for GM1/POPC (see Fig. S3). The more compact packing of ceramide can be regarded as a reason for this, since the hydrophilic head is much smaller. The large hydrophilic headgroup of GM1 obviously influences the phase behavior of the GM1/POPC system, but still allows for the formation of gel-like domains.

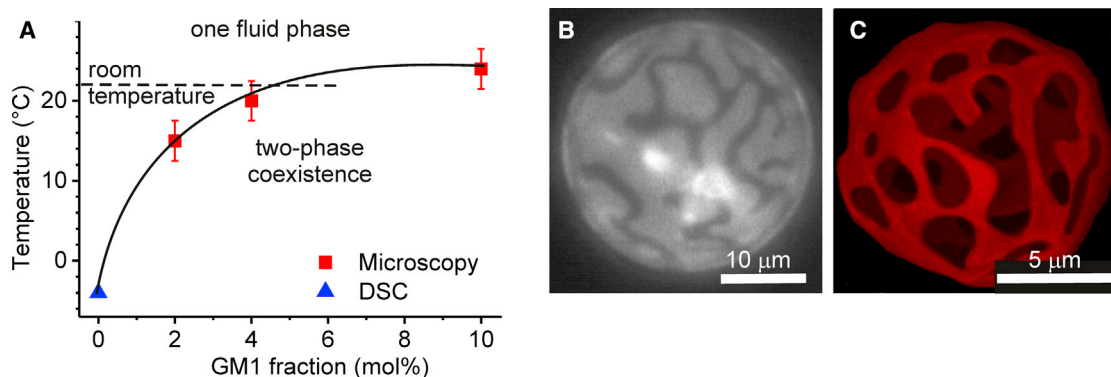


FIGURE 3 (A) Partial phase diagram of the POPC/GM1 system in 1 mM HEPES, deduced from fluorescence microscopy on GUVs. The solid triangle corresponds to available data for DSC measurements on pure POPC membranes. The error bars indicate the temperature ranges where different samples exhibit domain formation upon cooling. Errors in the GM1 fraction were not assessed, but desorption of the ganglioside, if present, will shift the binodal to the left. (B and C) GM1-rich gel-like domains (*dark*) at room temperature in a POPC-rich fluid environment (*bright*) visualized on GUVs containing (B) 8 mol % GM1 (imaged with epifluorescence) or (C) 10 mol % GM1 (whole-GUV three-dimensional reconstruction from confocal scans). The membrane was labeled with 0.1 mol % TR-DHPE.

In an attempt to characterize the nature and composition of the two phases observed here, we employed different fluorescent labels. The dye Bodipy-GM1 (tail labeled; see Fig. 2) is often used to locate GM1 in biomembranes and model membranes, and to track the function of the GM1 headgroup (54). A top view of a GUV marked with both Bodipy-GM1 and TR-DHPE is presented in Fig. 4, A–C. The fluorescence of Bodipy-GM1 colocalizes with that of TR-DHPE, suggesting that Bodipy-GM1 is excluded from the GM1-rich gel-like phase of the membrane. It was previously reported that the relatively bulky Bodipy probe does not enter the ordered phase (50). Obviously, Bodipy-GM1 cannot be used as a marker for the preferential partitioning of GM1 between the two phases observed here, presumably because of the difference between the hydrophobic moieties of GM1 and Bodipy-GM1 (Fig. 2).

Another obvious GM1 marker that we explored is the protein CTB, which exclusively binds to GM1. CTB, having five receptors for GM1, is extensively used to characterize ganglioside functions. The fluorescently labeled analog of this pentameric, ring-shaped molecule, CTB-Alexa, was dissolved in HEPES buffer and subsequently added to the GUV solution (at  $\sim 2.5 \mu\text{g/mL}$ ). Immediately after the addition, the GUVs exhibited CTB-Alexa fluorescence over the whole vesicle surface (data not shown). Presumably, the adsorption of the protein onto the membrane resulted in lipid redistribution in the bilayer, as was previously observed on supported lipid bilayers (55) and in multicomponent GUVs (56,57) (similar behavior was found upon

adsorption of the protein cytochrome *c* onto GUVs (58)). After a few minutes, the dark domains emerged again, but with some weak fluorescence in their center that was visible even after 15 min. An example of such a vesicle with dark domains and weak fluorescence in their center is shown in Fig. 4, D–F. The vesicle contained 8 mol % GM1 and was labeled with TR-DHPE, a marker for the fluid phase. A sharp distinction between both phases of the bilayer is visible, and colocalization of TR-DHPE and CTB-Alexa within the POPC-rich fluid phase can be observed. The weak fluorescence in the gel-like domains from adsorption of CTB-Alexa (see *green arrowheads* in Fig. 4 F) decreases with time and after  $\sim 60$  min is not detected due to bleaching of the Alexa dye, which is practically immobilized in the gel-like domains. Note that CTB does not appear to self-aggregate on membranes (59), and it is unlikely that the observed effect is due to nonspecific CTB aggregation at the vesicle surface.

The unusual fluorescence distribution and changes in domain structure (or domain presence) caused by CTB adsorption immediately after introduction of the protein indicate that CTB strongly influences the phase state of the membrane. This observation is corroborated by recent coarse-grained, dissipative particle dynamics simulations that suggested that when binding to gel-like (or interdigitated) membranes made of dioleoylphosphatidylcholine and GM1, CTB induces the formation of less-ordered nanodomains (where the toxin can even partially penetrate the membrane) (60). Consistent with our findings, the binding of the CTB-pentamer to GM1 was shown to alter the lateral mobility, lipid phase state, and chain organization of supported lipid bilayers (55). Presumably, the effects observed here result from cross-linking of GM1 molecules via the pentameric binding of CTB to them (56), which might lead to restructuring of the phases present in the GUVs. After equilibration, the gel-like domains reappear. This observation is confirmed by a report that CTB binding to supported lipid bilayers nucleates nanometer gel-phase domains with size propagating beyond the immediate binding site (55). We cannot exclude the possibility that the gel-like domains seen here in the presence of CTB-Alexa have a different composition compared with those observed in the absence of the protein. However, from the colocalization of TR-DHPE and CTB-Alexa fluorescence, we conclude that, similarly to Bodipy-GM1, CTB-Alexa is also not a marker that correctly visualizes the distribution of GM1 between the two phases.

The phase diagram in Fig. 3 A shows that at room temperature, the GM1-poor fluid phase present in the coexistence region contains 4–5 mol % of GM1. We were not able to determine the solidus line at high concentrations of GM1 because low temperatures were not accessible and vesicles with a high content of GM1 could not be prepared. However, a rough estimate of the gel-like phase composition can be made based on the domain area ratio and molecular

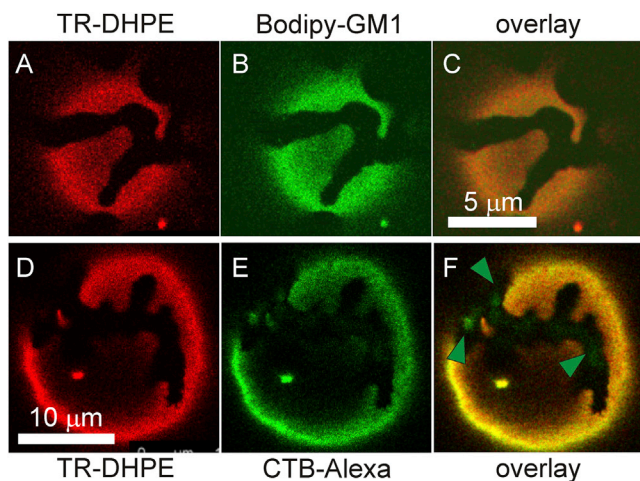


FIGURE 4 Domains visualized on two POPC vesicles doped with 8 mol % GM1 at 22°C. (A–C) In the upper row of images, the vesicle was labeled with TR-DHPE and Bodipy-GM1, and individual snapshots show the fluorescence in the respective channels and the overlay image. (D–F) In the lower row of images, the vesicle was labeled with TR-DHPE and exposed to CTB-Alexa added in the buffer. The individual snapshots show the fluorescence in the respective channels and the overlay image. The green arrowheads in (F) point to CTB-Alexa fluorescence detected in the interior of the gel-like domains. The images were obtained under the open pinhole of a confocal microscope.

areas of GM1 and POPC. The area fraction of the gel-like domains for GUVs containing 8 mol % GM1 was found to be between 10% and 15%, yielding 30–50 mol % for the fraction of GM1 in the gel-like domains (here, we assumed that no desorption of GM1 from the membrane had occurred). These values suggest that at such high fractions of GM1 in the gel-like domains, binding of CTB might be sterically hindered, as the distance between neighboring GM1 molecules might not fit the binding sites of CTB. Similar steric effects were observed with supported lipid bilayers (44) and with LUV and GUV samples (61), and were also related to the tendency of GM1 to cluster into complexes (44,62,63), which is favored by the formation of hydrogen bonds between the sugar groups of GM1 (64,65).

### Bending rigidity in the fluid phase

Administration of GM1 has been found to be beneficial for Parkinson patients (9), and the high fraction of GM1 in neurons has been correlated with their plasticity and axonal growth (see Ref. (4) and references therein). We thus evaluated the effect of this molecule on the membrane bending rigidity, the physical property that defines how easy it is to deform the neuronal membrane. The GM1-concentration dependence of the bending rigidity at 40°C, where the vesicle membrane is in the fluid phase for all compositions examined here, is shown in Fig. 5 A. The data were obtained from fluctuation analysis (*solid squares*) performed on more than 15 GUVs per composition. The bending rigidities obtained by vesicle electrodeformation (Fig. 5 A, *stars*) were measured only for pure POPC and for higher fractions of GM1. Micropipette aspiration measurements were hindered by strong evaporation in the open chamber at this temperature and are not presented.

The bending rigidity of pure POPC membranes measured via fluctuation analysis was found to be  $\kappa = (10.0 \pm 0.3) 10^{-20}$  J, which agrees well with values measured previously for this lipid (for an overview, see Ref. (26)). The presence of GM1 significantly softens the membrane. In the range between 2 and 7 mol % of GM1, the bending rigidity decreases almost linearly, whereas above 7 mol % it remains constant at  $(2.0 \pm 0.4) 10^{-20}$  J. As evidenced by the small uncertainties of the data in Fig. 5 A, the accuracy of the fluctuation analysis increases for smaller values of the bending rigidity, because the fluctuation amplitudes increase and can be measured more accurately.

Sterically, the GM1 molecule takes effectively more space than POPC in the membrane. Thus, the decrease of the rigidity at higher fractions of GM1 can be explained by the increase in the mean area per lipid and thus a decrease of the mean chain density in the membrane. Based on theoretical considerations, attached or embedded molecules can also reduce the effective bending rigidity of the membrane (66). Even at very low concentrations, inclusions can induce instabilities of the membrane curvature for both symmetric

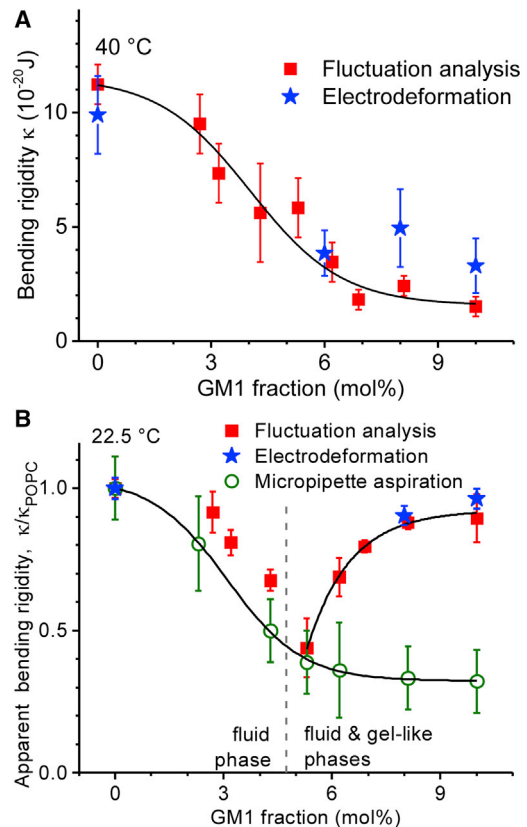


FIGURE 5 (A and B) Bending rigidity  $\kappa$  as a function of GM1 content, obtained by fluctuation analysis (*solid squares*; more than 15 vesicles per composition), electrodeformation (*stars*; 10 vesicles per composition), and micropipette aspiration (*open circles*; 5 vesicles per composition) at 40°C (A) and room temperature (B). The error bars represent the standard deviations. The data in (B) are rescaled by the bending rigidity of the pure POPC membrane measured at this temperature,  $\kappa_{\text{POPC}} \cong 9.4 \pm 1.5 \times 10^{-20}$  J. Note that the data in the two-phase region represent only the apparent bending rigidity, as the methods were not developed for vesicles with coexisting domains. The solid curves (sigmoidal fits) are guides for the eye. The dashed line in (B) tentatively illustrates the boundary between fluid phase and fluid-gel coexistence, as shown in the phase diagram in Fig. 3 A. To see this figure in color, go online.

(67) and asymmetric (68) distributions across the membrane, which experimentally manifest as larger fluctuations and a decrease in the measured effective bending rigidity. Sugars are also known to reduce the membrane rigidity of model membranes (25,26), so an influence of the sugar groups of GM1 could be expected as well. The observed softening of the membrane caused by GM1 may be easily envisioned to facilitate shape changes in neuronal membranes. In addition, domain formation driven by GM1 clustering presumably would be an important factor governing membrane morphology in general (69).

### Bending rigidity at room temperature

We examined the effect of GM1 content on the bending rigidity at room temperature (22°C) as well. Because at high

GM1 fractions the membrane exhibits coexistence of domains with very different rigidities, we will refer to the measured overall vesicle stiffness as the apparent bending rigidity. The influence of the glycolipid on the apparent bending rigidity of the POPC membrane at room temperature is shown in Fig. 5 B. Here, the method of micropipette aspiration was employed in addition to fluctuation analysis and electrodeformation. At GM1 fractions below 5 mol %, the membrane is in the fluid phase and the bending rigidity decreases with increasing GM1 content, as was found for measurements at high temperature (compare with data in Fig. 5 A). An increase in the GM1 fraction above 5 mol % leads to phase separation in the membrane (see Fig. 3 A) and the appearance of gel-like domains. Here, the results from fluctuation analysis (*solid squares* in Fig. 5 B) indicate stiffening of the membrane with increasing GM1 fractions. The fluctuation spectra of the membranes with domains do not appear to be influenced significantly by the presence of domains (see example in Fig. S4). Presumably, the short duration of the measurements (40–60 s) does not allow the gel-like domain segments in the equatorial section to affect the spectra significantly. One might be tempted to interpret the increased bending rigidity as a consequence of the combined or averaged stiffness of the fluid and gel phases. However, this interpretation is futile. On the one hand, the bending rigidity of gel-phase membranes is orders of magnitude higher than that of fluid ones (70). On the other hand, the influence of the boundaries between these two phases on the membrane fluctuations is not known.

For high fractions of GM1, the effective bending rigidity assessed by micropipette aspiration remains low, in contrast to the data obtained from fluctuation analysis and electrodeformation. Presumably, the aspiration method detects the bending rigidity of the fluid phase only because the sole contribution to the measured area change (which is needed to assess the bending rigidity) arises solely from smoothing of fluctuations of the fluid phase. The gel-like phase does not contribute, as it does not exhibit detectable fluctuations. In addition to this, the stiffer domains are not aspirated into the micropipette, as observed by fluorescence microscopy (data not shown). Indeed, the idea that the aspiration method assesses the bending rigidity of the fluid phase is further corroborated by the similarity in the trends of the aspiration-method data in Fig. 5 B and the data measured at 40°C in Fig. 5 A. Furthermore, in the high-GM1-fraction regime, the bending rigidity of the fluid phase should remain constant (as indicated by the *open circles* in Fig. 5 B) because in the phase-coexistence region, the composition of the fluid phase remains constant, as defined by the horizontal tie lines in the two-component mixtures.

Similarly to the results obtained via fluctuation analysis for high-GM1 fractions, the data acquired from electrodeformation of vesicles show bending rigidities larger than those deduced from micropipette aspiration. We speculate

that the stiff gel-phase domains suppress the overall vesicle deformation, making the membrane appear more rigid.

## CONCLUSIONS

In this work, we performed systematic studies to assess the influence of GM1 on the phase behavior, charge, and elasticity of POPC membranes. Since GM1 carries a negative charge, we used electrophoretic measurements to confirm the membrane composition in the vesicles. The data suggest that both GM1 and POPC bear a constant electric charge independently of the membrane composition.

At room temperature, high fractions of GM1 were found to induce phase separation of the membrane. Fluorescence-microscopy observations showed the presence of GM1-rich, dendritic-shaped domains of a gel-like phase, which moved freely in the liquid POPC-rich phase. To our knowledge, this study is the first to show the presence of microscopic, GM1-rich, gel-like domains in this system. The fluorescence microscopy data were used to build a partial phase diagram of the system (Fig. 3 A). The fluorescent molecules GM1-Bodipy and CTB-Alexa, which are typically used as markers for GM1, were shown to incorrectly report the partitioning of the ganglioside between the domains. The dense populations of GM1 in the gel-like domains were found to limit the functionality of the ganglioside as a receptor for CTB.

We assessed the bending rigidity of GM1-doped membranes using three different methods: fluctuation analysis, electrodeformation, and micropipette aspiration. We proposed a simplified approach for conducting and analyzing the experimental data obtained with the method of vesicle electrodeformation (see Eq. 2). This approach offers experimentalists a relatively easy and undemanding solution for assessing the bending rigidity of membranes. Using fluctuation analysis, the influence of GM1 on the bending rigidity of the nonphase-separated bilayer was found to decrease with increasing GM1 content. The appearance of gel-like domains was seen as an apparent stiffening of the membrane, detected both by fluctuation spectroscopy and with the method of vesicle electrodeformation. Presumably, to study the applicability of these methods to vesicles with gel-like domains in greater detail, one would have to visualize these domains simultaneously at the equator during contour acquisition. Micropipette aspiration measurements on vesicles with gel-like domains appeared to detect the bending rigidity of the fluid phase only (Fig. 5 B).

An increasing number of studies are employing GM1-doped giant vesicles as a means of characterizing the phase state of the membrane and the performance of proteins that interact with it (see, e.g., Refs. (46,47,71–74)). Our studies exploring the low-concentration range of GM1 and, in particular, the finding that phase separation occurs at very small mole fractions of the ganglioside in the membrane, point to the importance of characterizing the effect of GM1 on the thermodynamic properties of the membrane

before examining any interactions. The strong decrease of the membrane bending rigidity induced by small fractions of GM1 is also relevant to understanding the vesicle morphological changes observed in the above-cited studies. What remains largely unexplored is the effect of GM1 on membranes containing cholesterol. The results regarding the bilayer bending rigidity are also important for understanding the role of this ganglioside in the flexibility of neuronal membranes. Our data suggest that GM1 plays one more function in addition to the numerous tasks it has already been found to undertake (10). Bilayer softening by GM1 strongly facilitates membrane deformations and may help to elucidate the mechanisms involved in neurite sprouting (13) and neuronal growth and development (10,12). The latter processes entail bending of the membrane into highly curved tubular structures, which would be energetically costly if the bending rigidity of the bilayer was high. The correlation between the high fraction of GM1 in neurons and their plasticity and axonal growth (4) might well be related to the softening that this ganglioside confers to membranes. Local concentration differences in the distribution of GM1 along the membrane (that might also induce local stiffening if gel-like domains form) may efficiently modulate the membrane shape. In addition, being asymmetrically distributed across the membrane, the ganglioside may strongly affect the spontaneous curvature of neuronal membranes. In our current experimental efforts, we are attempting to address the contribution of such an asymmetry.

## SUPPORTING MATERIAL

Supporting Material and four figures are available at [http://www.biophysj.org/biophysj/supplemental/S0006-3495\(16\)30829-3](http://www.biophysj.org/biophysj/supplemental/S0006-3495(16)30829-3).

## AUTHOR CONTRIBUTIONS

N.F. and R.D. designed the experiments and wrote the manuscript. N.F. performed the experiments.

## ACKNOWLEDGMENTS

We thank C. Remde for assistance with the DCS and electrophoresis measurements, K. Riske for consultation regarding analysis of the DSC data, J. Steinkühler and T. Bhatia for help with the phase transition studies on giant vesicles, and V. Georgiev for help in drawing the molecule structures.

## REFERENCES

1. Seeberger, P. H., and D. B. Werz. 2007. Synthesis and medical applications of oligosaccharides. *Nature*. 446:1046–1051.
2. Zhang, S., C. Cordon-Cardo, ..., P. O. Livingston. 1997. Selection of tumor antigens as targets for immune attack using immunohistochemistry: I. Focus on gangliosides. *Int. J. Cancer*. 73:42–49.
3. Thompson, T. E., and T. W. Tillack. 1985. Organization of glycosphingolipids in bilayers and plasma membranes of mammalian cells. *Annu. Rev. Biophys. Chem.* 14:361–386.
4. Skaper, S. D., S. Mazzari, ..., A. Leon. 1991. Monosialoganglioside GM1 and modulation of neuronal plasticity in CNS repair processes. *In* Plasticity and Regeneration of the Nervous System. P. Timiras, A. Privat, E. Giacobini, J. Lauder, and A. Vernadakis, editors. Springer, New York, pp. 257–266.
5. Hakomori, S. 1993. Structure and function of sphingoglycolipids in transmembrane signalling and cell-cell interactions. *Biochem. Soc. Trans.* 21:583–595.
6. Hakomori, S. I. 2000. Cell adhesion/recognition and signal transduction through glycosphingolipid microdomain. *Glycoconj. J.* 17: 143–151.
7. Derry, D. M., and L. S. Wolfe. 1967. Gangliosides in isolated neurons and glial cells. *Science*. 158:1450–1452.
8. Maggio, B. 1994. The surface behavior of glycosphingolipids in biomembranes: a new frontier of molecular ecology. *Prog. Biophys. Mol. Biol.* 62:55–117.
9. Schneider, J. S., F. Cambi, ..., D. F. Wong. 2015. GM1 ganglioside in Parkinson's disease: pilot study of effects on dopamine transporter binding. *J. Neurol. Sci.* 356:118–123.
10. Ledeen, R. W., and G. Wu. 2015. The multi-tasked life of GM1 ganglioside, a true factotum of nature. *Trends Biochem. Sci.* 40:407–418.
11. Cantu, L., M. Corti, ..., E. Del Favero. 2009. Structural aspects of ganglioside-containing membranes. *Biochim. Biophys. Acta.* 1788: 202–208.
12. Skaper, S. D., A. Leon, and G. Toffano. 1989. Ganglioside function in the development and repair of the nervous system. From basic science to clinical application. *Mol. Neurobiol.* 3:173–199.
13. Roisen, F. J., H. Bartfeld, ..., G. Yorke. 1981. Ganglioside stimulation of axonal sprouting in vitro. *Science*. 214:577–578.
14. Dimova, R. 2012. Giant vesicles: a biomimetic tool for membrane characterization. *In* Advances in Planar Lipid Bilayers and Liposomes. A. Iglič, editor. Academic Press, New York, pp. 1–50.
15. Dimova, R., S. Aranda, ..., R. Lipowsky. 2006. A practical guide to giant vesicles. Probing the membrane nanoregime via optical microscopy. *J. Phys. Condens. Matter*: 18:S1151–S1176.
16. Henriksen, J., A. C. Rowat, and J. H. Ipsen. 2004. Vesicle fluctuation analysis of the effects of sterols on membrane bending rigidity. *Eur. Biophys. J.* 33:732–741.
17. Gracià, R. S., N. Bezlyepkina, ..., R. Dimova. 2010. Effect of cholesterol on the rigidity of saturated and unsaturated membranes: fluctuation and electrodeformation analysis of giant vesicles. *Soft Matter*. 6:1472–1482.
18. Shchelokovskyy, P., S. Tristram-Nagle, and R. Dimova. 2011. Effect of the HIV-1 fusion peptide on the mechanical properties and leaflet coupling of lipid bilayers. *New J. Phys.* 13:25004.
19. Evans, E., and W. Rawicz. 1990. Entropy-driven tension and bending elasticity in condensed-fluid membranes. *Phys. Rev. Lett.* 64:2094–2097.
20. Henriksen, J. R., and J. H. Ipsen. 2004. Measurement of membrane elasticity by micro-pipette aspiration. *Eur Phys J E Soft Matter*. 14:149–167.
21. Kummrow, M., and W. Helfrich. 1991. Deformation of giant lipid vesicles by electric fields. *Phys. Rev. A*. 44:8356–8360.
22. Niggemann, G., M. Kummrow, and W. Helfrich. 1995. The bending rigidity of phosphatidylcholine bilayers: dependences on experimental method, sample cell sealing and temperature. *J. Phys. II*. 5:413–425.
23. Angelova, M. I., and D. S. Dimitrov. 1986. Liposome electroformation. *Faraday Discuss.* 81:303–311.
24. Andersen, H. D., C. Wang, ..., P. Westh. 2011. Reconciliation of opposing views on membrane-sugar interactions. *Proc. Natl. Acad. Sci. USA*. 108:1874–1878.
25. Vitkova, V., and A. G. Petrov. 2013. Lipid bilayers and membranes: material properties. *In* Advances in Planar Lipid Bilayers and Liposomes. A. Iglič and J. Genova, editors. Academic Press, New York, pp. 89–138.

26. Dimova, R. 2014. Recent developments in the field of bending rigidity measurements on membranes. *Adv. Colloid Interface Sci.* 208: 225–234.
27. Henriksen, J. R., and J. H. Ipsen. 2002. Thermal undulations of quasi-spherical vesicles stabilized by gravity. *Eur Phys J E Soft Matter.* 9:365–374.
28. Kwok, R., and E. Evans. 1981. Thermoelasticity of large lecithin bilayer vesicles. *Biophys. J.* 35:637–652.
29. Evans, E., and W. Rawicz. 1997. Elasticity of “fuzzy” biomembranes. *Phys. Rev. Lett.* 79:2379–2382.
30. Yamamoto, T., S. Aranda-Espinoza, ..., R. Lipowsky. 2010. Stability of spherical vesicles in electric fields. *Langmuir.* 26:12390–12407.
31. Klasczyk, B., V. Knecht, ..., R. Dimova. 2010. Interactions of alkali metal chlorides with phosphatidylcholine vesicles. *Langmuir.* 26: 18951–18958.
32. Dimova, R., N. Bezlyepkina, ..., R. Lipowsky. 2009. Vesicles in electric fields: some novel aspects of membrane behavior. *Soft Matter.* 5:3201–3212.
33. Aranda, S., K. A. Riske, ..., R. Dimova. 2008. Morphological transitions of vesicles induced by alternating electric fields. *Biophys. J.* 95:L19–L21.
34. Staykova, M., R. Lipowsky, and R. Dimova. 2008. Membrane flow patterns in multicomponent giant vesicles induced by alternating electric fields. *Soft Matter.* 4:2168–2171.
35. Vitkova, V., J. Genova, and I. Bivas. 2004. Permeability and the hidden area of lipid bilayers. *Eur. Biophys. J.* 33:706–714.
36. Rodriguez, N., F. Pincet, and S. Cribier. 2005. Giant vesicles formed by gentle hydration and electroformation: a comparison by fluorescence microscopy. *Colloids Surf. B Biointerfaces.* 42:125–130.
37. Cevc, G. 1993. Electrostatic characterization of liposomes. *Chem. Phys. Lipids.* 64:163–186.
38. McLaughlin, S. 1989. The electrostatic properties of membranes. *Annu. Rev. Biophys. Biophys. Chem.* 18:113–136.
39. Lyklema, J. 2005. *Fundamentals of Interface and Colloid Science: Soft Colloids.* Academic Press, New York.
40. McDaniel, R. V., A. McLaughlin, ..., S. McLaughlin. 1984. Bilayer membranes containing the ganglioside GM1: models for electrostatic potentials adjacent to biological membranes. *Biochemistry.* 23:4618–4624.
41. Kučerka, N., S. Tristram-Nagle, and J. F. Nagle. 2005. Structure of fully hydrated fluid phase lipid bilayers with monounsaturated chains. *J. Membr. Biol.* 208:193–202.
42. Corti, M., V. Degiorgio, ..., G. Tettamanti. 1980. Laser-light scattering investigation of the micellar properties of gangliosides. *Chem. Phys. Lipids.* 26:225–238.
43. Maggio, B., T. Ariga, ..., R. K. Yu. 1985. Thermotropic behavior of glycosphingolipids in aqueous dispersions. *Biochemistry.* 24: 1084–1092.
44. Shi, J., T. Yang, ..., P. S. Cremer. 2007. GM1 clustering inhibits cholera toxin binding in supported phospholipid membranes. *J. Am. Chem. Soc.* 129:5954–5961.
45. Kubsch, B., T. Robinson, ..., R. Dimova. 2016. Solution asymmetry and salt expand fluid-fluid coexistence regions of charged membranes. *Biophys. J.* 110:2581–2584.
46. Ewers, H., W. Römer, ..., L. Johannes. 2010. GM1 structure determines SV40-induced membrane invagination and infection. *Nat. Cell Biol.* 12:11–18, 1–12.
47. Dietrich, C., L. A. Bagatolli, ..., E. Gratton. 2001. Lipid rafts reconstituted in model membranes. *Biophys. J.* 80:1417–1428.
48. Frey, S. L., E. Y. Chi, ..., K. Y. C. Lee. 2008. Condensing and fluidizing effects of ganglioside GM1 on phospholipid films. *Biophys. J.* 94:3047–3064.
49. Yuan, C., and L. J. Johnston. 2001. Atomic force microscopy studies of ganglioside GM1 domains in phosphatidylcholine and phosphatidylcholine/cholesterol bilayers. *Biophys. J.* 81:1059–1069.
50. Burns, A. R., D. J. Frankel, and T. Buranda. 2005. Local mobility in lipid domains of supported bilayers characterized by atomic force microscopy and fluorescence correlation spectroscopy. *Biophys. J.* 89:1081–1093.
51. Rock, P., M. Allietta, ..., T. W. Tillack. 1991. Ganglioside GM1 and asialo-GM1 at low concentration are preferentially incorporated into the gel phase in two-component, two-phase phosphatidylcholine bilayers. *Biochemistry.* 30:19–25.
52. Goni, F. M., and A. Alonso. 2006. Biophysics of sphingolipids I. Membrane properties of sphingosine, ceramides and other simple sphingolipids. *Biochim. Biophys. Acta.* 1758:1902–1921.
53. Silva, L., R. F. M. de Almeida, ..., M. Prieto. 2006. Ceramide-platform formation and -induced biophysical changes in a fluid phospholipid membrane. *Mol. Membr. Biol.* 23:137–148.
54. Coban, O., M. Burger, ..., L. J. Johnston. 2007. Ganglioside partitioning and aggregation in phase-separated monolayers characterized by Bodipy GM1 monomer/dimer emission. *Langmuir.* 23:6704–6711.
55. Forstner, M. B., C. K. Yee, ..., J. T. Groves. 2006. Lipid lateral mobility and membrane phase structure modulation by protein binding. *J. Am. Chem. Soc.* 128:15221–15227.
56. Hammond, A. T., F. A. Heberle, ..., G. W. Feigenson. 2005. Crosslinking a lipid raft component triggers liquid ordered-liquid disordered phase separation in model plasma membranes. *Proc. Natl. Acad. Sci. USA.* 102:6320–6325.
57. Bacia, K., P. Schwille, and T. Kurzchalia. 2005. Sterol structure determines the separation of phases and the curvature of the liquid-ordered phase in model membranes. *Proc. Natl. Acad. Sci. USA.* 102:3272–3277.
58. Patariaia, S., Y. G. Liu, ..., R. Dimova. 2014. Effect of cytochrome *c* on the phase behavior of charged multicomponent lipid membranes. *Biochim. Biophys. Acta.* 1838:2036–2045.
59. Cai, X.-E., and J. Yang. 2003. The binding potential between the cholera toxin B-oligomer and its receptor. *Biochemistry.* 42:4028–4034.
60. Sun, H., L. Chen, ..., W. Fang. 2015. Nanodomain formation of ganglioside GM1 in lipid membrane: effects of cholera toxin-mediated cross-linking. *Langmuir.* 31:9105–9114.
61. Šachl, R., M. Amaro, ..., M. Hof. 2015. On multivalent receptor activity of GM1 in cholesterol containing membranes. *Biochim. Biophys. Acta.* 1853:850–857.
62. Cantù, L., M. Corti, ..., G. Tettamanti. 1996. Experimental evidence of a temperature-related conformational change of the hydrophilic portion of gangliosides. *Chem. Phys. Lipids.* 79:137–145.
63. Marushchak, D., N. Gretskaya, ..., L. B. A. Johansson. 2007. Self-aggregation—an intrinsic property of G(M1) in lipid bilayers. *Mol. Membr. Biol.* 24:102–112.
64. Bertoli, E., M. Masserini, ..., G. Tettamanti. 1981. Electron paramagnetic resonance studies on the fluidity and surface dynamics of egg phosphatidylcholine vesicles containing gangliosides. *Biochim. Biophys. Acta.* 647:196–202.
65. Manna, M., T. Rog, and I. Vattulainen. 2014. The challenges of understanding glycolipid functions: an open outlook based on molecular simulations. *Biochim. Biophys. Acta.* 1841:1130–1145.
66. Bivas, I., and P. Méléard. 2003. Bending elasticity and bending fluctuations of lipid bilayer containing an additive. *Phys. Rev. E Stat. Nonlin. Soft Matter Phys.* 67:012901.
67. Leibler, S. 1986. Curvature instability in membranes. *J. Phys.* 47: 507–516.
68. Fournier, J. B. 1996. Nontopological saddle-splay and curvature instabilities from anisotropic membrane inclusions. *Phys. Rev. Lett.* 76:4436–4439.
69. Lipowsky, R., and R. Dimova. 2003. Domains in membranes and vesicles. *J. Phys. Condens. Matter.* 15:S31–S45.
70. Dimova, R., B. Pouligny, and C. Dietrich. 2000. Pretransitional effects in dimyristoylphosphatidylcholine vesicle membranes: optical dynamometry study. *Biophys. J.* 79:340–356.

71. Roux, A., D. Cuvelier, ..., B. Goud. 2005. Role of curvature and phase transition in lipid sorting and fission of membrane tubules. *EMBO J.* 24:1537–1545.
72. Sorre, B., A. Callan-Jones, ..., P. Bassereau. 2009. Curvature-driven lipid sorting needs proximity to a demixing point and is aided by proteins. *Proc. Natl. Acad. Sci. USA.* 106:5622–5626.
73. Puff, N., C. Watanabe, ..., G. Staneva. 2014. Lo/Ld phase coexistence modulation induced by GM1. *Biochim. Biophys. Acta.* 1838:2105–2114.
74. Garten, M., C. Prévost, ..., S. Vanni. 2015. Methyl-branched lipids promote the membrane adsorption of  $\alpha$ -synuclein by enhancing shallow lipid-packing defects. *Phys. Chem. Chem. Phys.* 17:15589–15597.

## SUPPORTING INFORMATION

### Text S1. Assessing the membrane tension in vesicles exposed to electrodeformation

The force density  $f$  arising from the accumulation of electric charge at both interfaces of the membrane acts as a local pressure on the membrane in addition to the pressure difference  $\Delta p$  between the interior and exterior of the vesicles as described by the Young-Laplace equation. At the poles (pol) and at the equator (equ), the force balance between pressure and tension has the form  $2M_{\text{pol}}\Sigma = \Delta p + f_{\text{pol}}$  and  $2M_{\text{equ}}\Sigma = \Delta p + f_{\text{equ}}$ , where  $M_{\text{pol}}$  and  $M_{\text{equ}}$  are the mean curvatures of the membrane at the poles and equator, respectively, and  $f_{\text{pol}}$  and  $f_{\text{equ}}$  are the respective force densities. By eliminating the osmotic pressure from these equations, one can obtain for the tension  $\Sigma$  of the vesicle

$$\Sigma = \frac{f_{\text{pol}} - f_{\text{equ}}}{2(M_{\text{pol}} - M_{\text{equ}})}$$

Full derivation of the force densities  $f_{\text{pol}}$  and  $f_{\text{equ}}$  can be found in Ref. (1), Appendix B (Ref. 30 in the main text). Here, we use the same notations. The resulting force densities for each angle  $\theta$  along the vesicle are the superposition of the radial Maxwell stresses directed to the exterior, the bilayer and the interior of the vesicle, denoted as 1, 2 and 3 in the indices, respectively, at the exterior (ex) and interior (in) interface:

$$f(\theta) = [T_{1rr}(r_{\text{ex}}, \theta) - T_{2rr}(r_{\text{ex}}, \theta)] + [T_{2rr}(r_{\text{in}}, \theta) - T_{3rr}(r_{\text{in}}, \theta)]$$

where  $r_{\text{ex}}$  and  $r_{\text{in}}$  describe the outer and inner radius of the vesicle.

Following equations 84 and 85 in Ref. (1), the radial components of the stresses that may cause a deformation at the exterior interface are:

$$T_{1rr}(r_{\text{ex}}, \theta) = \frac{1}{4} \epsilon_1 E_0^2 [|\alpha_{1,\text{ex}}|^2 \cos^2 \theta - |\gamma_{\text{ex}}|^2 \sin^2 \theta]$$

$$T_{2rr}(r_{\text{ex}}, \theta) = \frac{1}{4} \epsilon_2 E_0^2 [|\alpha_{2,\text{ex}}|^2 \cos^2 \theta - |\gamma_{\text{ex}}|^2 \sin^2 \theta]$$

and at the interior interface (following equations 88 and 89 in Ref. (1):

$$T_{2rr}(r_{\text{in}}, \theta) = \frac{1}{4} \epsilon_2 E_0^2 [|\alpha_{2,\text{in}}|^2 \cos^2 \theta - |\gamma_{\text{in}}|^2 \sin^2 \theta]$$

$$T_{3rr}(r_{\text{in}}, \theta) = \frac{1}{4} \epsilon_3 E_0^2 [|\alpha_{3,\text{in}}|^2 \cos^2 \theta - |\gamma_{\text{in}}|^2 \sin^2 \theta]$$

Here the amplitudes at the exterior (equations 65, 66 and 68 in Ref. (1)) and at the interior interface (equations 70, 71 and 73 Ref. (1)) are:

$$\begin{aligned} \alpha_{1,\text{ex}} &= \beta_1 \alpha_{2,\text{ex}} & \alpha_{2,\text{in}} &= 9/D \\ \alpha_{2,\text{ex}} &= 3[(1 + 2\beta_3) + 2(1 - \beta_3) \frac{r_{\text{in}}^3}{r_{\text{ex}}^3}] / D & \alpha_{3,\text{in}} &= \beta_3 \alpha_{2,\text{in}} \\ \gamma_{\text{ex}} &= -3 \left[ (1 + 2\beta_3) - (1 - \beta_3) \frac{r_{\text{in}}^3}{r_{\text{ex}}^3} \right] / D & \gamma_{\text{in}} &= -\alpha_{3,\text{in}} \end{aligned}$$

with the denominator

$$D = (2 - \beta_1)(1 + 2\beta_3) - 2(1 - \beta_1)(1 - \beta_3) \frac{r_{\text{in}}^3}{r_{\text{ex}}^3},$$

the complex-value electric parameters

$$\beta_1 = \frac{\sigma_2 - i\omega\epsilon_2}{\sigma_1 - i\omega\epsilon_1}, \quad \beta_3 = \frac{\sigma_2 - i\omega\epsilon_2}{\sigma_3 - i\omega\epsilon_3}$$

and the conductivities  $\sigma_{1,2,3}$ , the dielectric permittivities  $\epsilon_{1,2,3}$  and the circular electric frequency  $\omega$ .

At the poles ( $\theta = 90^\circ$ ) and equator ( $\theta = 0^\circ$ ), the force densities are then defined as:

$$f_{\text{pol}} = \frac{1}{4} E_0^2 \left[ (\epsilon_1 |\beta_1|^2 - \epsilon_2) |\alpha_{2,\text{ex}}|^2 + (\epsilon_2 - \epsilon_3 |\beta_3|^2) |\alpha_{2,\text{in}}|^2 \right]$$

$$f_{\text{equ}} = -\frac{1}{4} E_0^2 [(\epsilon_1 - \epsilon_2) |\gamma_{\text{ex}}|^2 + (\epsilon_2 - \epsilon_3) |\gamma_{\text{in}}|^2]$$

The terms in the square brackets are invariable during the experiment leading to the following dependence for the membrane tension

$$\Sigma = \frac{\text{const } E_0^2}{(M_{\text{pol}} - M_{\text{equ}})}$$

where *const* is a dimensional constant. Then, from the logarithmic expression for the relative area change in Eq. 1 in the main text, one obtains the simplified expression in Eq. 2 in the main text.

An approximation for working at “small” field frequencies  $\omega$  and low conductivities of the solutions  $\sigma_{1,3} \gg \sigma_2$  and  $|\beta_{1,3}| \ll 1 - (r_{\text{in}}/r_{\text{ex}})^3$  leads to:

$$\alpha_{2,\text{in}} \rightarrow \frac{9}{2 \left(1 - \frac{r_{\text{in}}^3}{r_{\text{ex}}^3}\right)}, \quad \alpha_{2,\text{ex}} \rightarrow \alpha_{2,\text{in}} - 3, \quad \gamma_{\text{in}} \rightarrow 0, \quad \gamma_{\text{ex}} \rightarrow -\frac{3}{2}$$

yielding for the forces

$$f_{\text{pol}} \rightarrow \frac{1}{4} \epsilon_2 E_0^2 \left( \frac{27}{1 - \frac{r_{\text{in}}^3}{r_{\text{ex}}^3}} - 9 \right) \text{ and } f_{\text{equ}} \rightarrow -\frac{9}{16} \epsilon_1 E_0^2$$

From these simplified expressions, the actual membrane tension during electrodeformation can be also assessed.

**Figure S1**

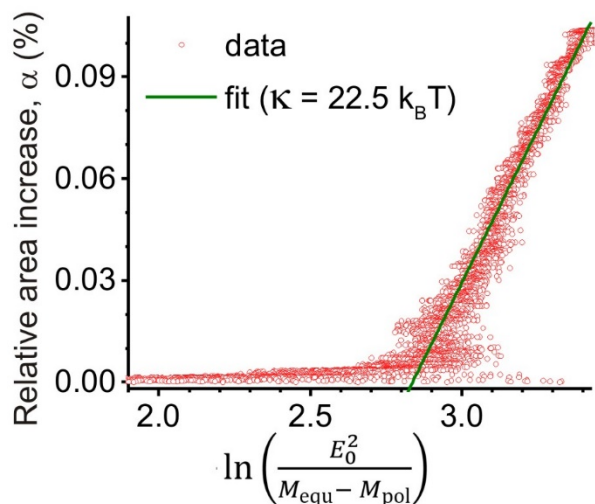


Figure S1. Change in the area of a POPC vesicle at 40 °C as a function of applied electric field strength (in V/m units) as measured in an electrodeformation experiment (the curvatures were measured in units 1/m). From the slope of the data, one obtains the bending rigidity following Eq. 2 in the main text.

**Figure S2**

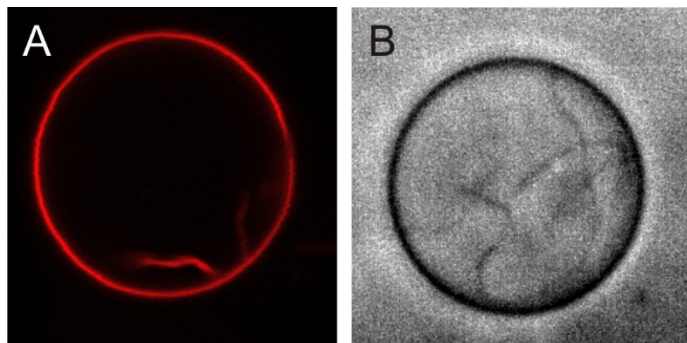
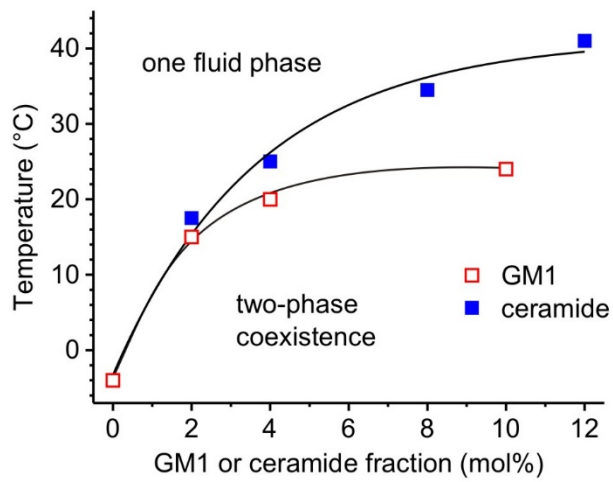


Figure S2. Images of vesicles with internal structures observed at room temperature for GM1 fractions of (A) 5.3 mol% (confocal cross section,) and (B) 10 mol% (phase contrast). The vesicle diameters are approximately (A) 35  $\mu\text{m}$  and (B) 25  $\mu\text{m}$ .

**Figure S3**



**Figure S3.** Partial phase diagram of POPC with palmitoyl ceramide (filled squares) or with GM1 (open squares). The data for GM1 is identical to that in Fig. 3A in the main text. The data for the POPC/palmitoyl ceramide system is from Ref. (2) (Ref. 54 in the main text). The solid curves are guides to the eye.

**Figure S4**

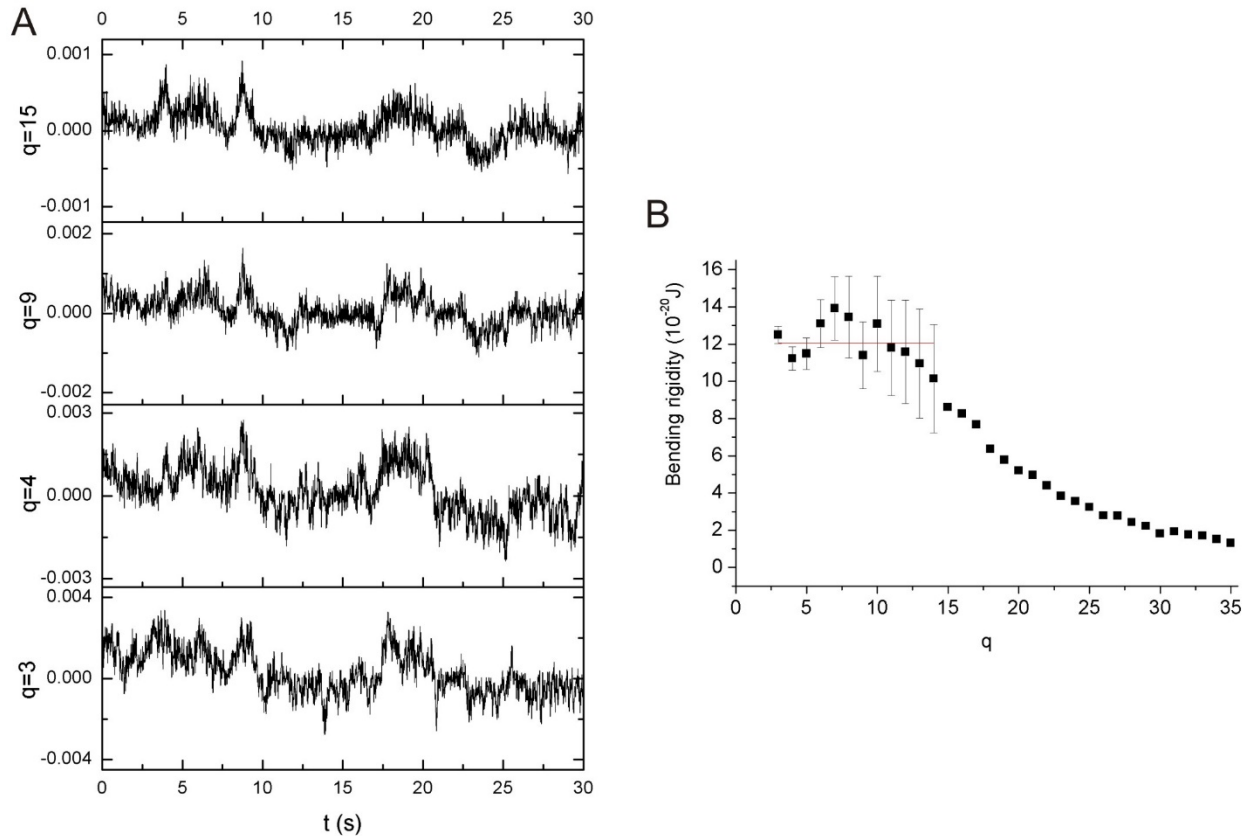


**Figure S4.** Example data for fluctuation analysis on vesicles with gel-like domains. The analysis is done following the approach in Ref. (3). The data was acquired on a vesicle with 8 mol% GM1 at room temperature. (A) Absolute values of the Fourier coefficients  $|v_q|$  for several of the modes  $q$  with subtracted mean value. (B) Fit for the bending rigidity deduced for the same vesicle,  $\kappa = 12.1 \pm 3.3 \times 10^{-20}$  J.

### References

1. Yamamoto, T., S. Aranda-Espinoza, R. Dimova, and R. Lipowsky. 2010. Stability of Spherical Vesicles in Electric Fields. *Langmuir* 26:12390-12407.
2. Silva, L., R. F. M. De Almeida, A. Fedorov, A. P. A. Matos, and M. Prieto. 2006. Ceramide-platform formation and -induced biophysical changes in a fluid phospholipid membrane. *Mol. Membr. Biol.* 23:137-U132.
3. Gracià, R. S., N. Bezlyepkina, R. L. Knorr, R. Lipowsky, and R. Dimova. 2010. Effect of cholesterol on the rigidity of saturated and unsaturated membranes: fluctuation and electrodeformation analysis of giant vesicles. *Soft Matter* 6:1472-1482.